Investigation of Nonlinear Behaviors of Packaging Materials and Its Application to a Flip-Chip Package

W. Ren, J. Wang, Z. Qian, D. Zou and S. Liu
Department of Mechanical Engineering
Wayne State University, Detroit, MI 48202

Abstract

The creep behavior of a flip-chip package under a thermal load is studied in this paper using different finite element models coupled with high density laser moiré interferometry. The accuracy of the results obtained from finite element analysis (FEA) strongly depends on the reliable input material database. Therefore, a series of tests are first carried out using a computer controlled 6-axis mini fatigue tester for both eutectic solder alloy 63Sn37Pb and underfill FP4526. Based on these reliable and consistent test data, six finite element models are used to simulate the creep deformation under the consideration of elastic, elastic-plastic, viscoelastic or viscoplastic behaviors for both solder balls and underfill. The results show that solder and underfill nonlinear material behaviors do not have significant effect on the warpage of the flip-chip, but do have significant effect on the stresses. It is found that in all visco FEA models the Von Mises stresses at the corner or at the center of the outmost solder ball greatly decrease. However, the Von Mises stresses predicted by elastic-plastic model and elastic model remain unchanged during the temperature holding time and are much higher than those achieved from visco FEA models. Although the stress values predicted by all visco models for the solder ball at the prescribed locations have no big difference, it is not true for underfill. By comparing with the results obtained from different FEA models, it is suggested that the strain rate-dependent model be used to well describe the creep behavior of underfill. On the other hand, the inelastic equivalent strain which is usually used as main parameter for the fatigue life prediction also have big difference due to different FEA models. Therefore, it is suggested that the suitable model be carefully chosen in order to be able to obtain accurate fatigue life prediction. Furthermore, the creep deformation for the same flip-chip package is measured by real-time moiré interferometry technique. The predicted deformation values of the flip-chip package obtained from all finite element models are compared with the test data obtained from the laser moiré interferometry technique. It is shown that the deformation values of the flip-chip package obtained from the finite element analysis are in a good agreement with those obtained from the test.

INTRODUCTION

Advanced microelectronic packaging requires higher I/O density and reliable interconnection technology to achieve higher levels of system performance at a competitive cost. To satisfy this demand, the flip-chip has now been widely used in the automotive, avionics, computers, and mobile electronics. However, the difference in the coefficients of thermal expansion (CTE) between the chip and the substrate makes flip-chip configurations vulnerable to thermally-induced strains and can potentially lead to the temperature dependent viscoplastic deformation in and around flip-chip solder joints. It often results in solder joint creep and fatigue (Lau, 1994; Lau and Pao, 1997). Therefore, further understanding the creep behavior and precisely predicting the creep and potentially cyclic behaviors of a flip-chip package are critically important for the reliability of electronic devices.

As the interconnections become smaller and smaller, it is clear that direct experimental measurement of the thermal strains (stresses) is extremely difficult. The experimental tools for deformation measurement can not offer enough resolution for local strain (stress) distributions which are essential for the estimation of reliability. On the other hand, measuring time-dependent deformation behaviors of electronic packages are usually time-consuming. Therefore, recently more and more effects have been made on the reliability study by using numerical method such as finite element method (Wang *et al.*, 1998; Lau and Pao, 1997, Bor Zen Hong *et al.*, 1996, only list a few). However, due to the lack of accurate, detailed viscoplastic material

properties for both underfill and solder alloy, the studies mainly emphasize the effect of mismatch of thermal expansion and neglect the viscoplastic nature of the encapsulant (Zhao *et al.*, 1998, Pang *et al.*, 1998) and sometime solder balls (Gektin *et al.*, 1997, Darbha, *et al.* , 1997). However, as described in authors' previous papers (Ren *et al.* 1997, Ren *et al.* 1998, Qian *et al.* 1998), the solder alloy shows strong viscoplastic nature even at room temperature. And the underfill also exhibits the strong viscolpastic behavior at the elevated temperature environment in which the package is usually subjected in the operation. Therefore, it may cause some error in the finite element analysis if the visco nature for both solder and underfill or only for the underfill is neglected. The knowledge of the visco behavior in the flip-chip package is an essential step to approach the precise reliability prediction. In addition, the finite element modeling coupled with the experimental study of the creep behavior of flip-chip packages under elevated temperatures by the real time moiré interferometry technique remains scarce.

In this paper a flip-ship package which is composed of silicon chip, underfill, solder balls and a FR-4 substrate is studied. Different constitutive laws, including elastic, elastic-plastic, viscoelastic or viscoplastic for both solder balls and underfill, are used to investigate the creep behaviors of flip-chip package coupled by the real time moiré interferometry technique.

FINITE ELEMENT MODELS AND MATERIAL PROPERTIES

The subject under investigation is a flip-chip package specimen. The dimensions and boundary conditions are shown in Figure 1. The thickness of the flip-chip specimen is 3.25mm. Assume the flip-chip package specimen satisfies the axisymmetric condition. Therefore, it can be simplified to be a 2D axisymmetric FEA model. A finite element mesh is shown in Figure 2. It is noted that a fine local mesh is arranged along all interfaces. In the analysis, the commercial code ABAQUS is applied and the eight-node element, CAX8 in ABAQUS, is selected. Two stages of analyses are performed in the current study. First the flip-chip specimen is heated up from room temperature to 115°C. Subsequently, the specimen undergoes the creep at 115°C for about 10 hours and 40 minutes. The temperature profile is illustrated in Figure 3.

The properties of the silicon chip and the substrate are assumed to be linear elastic. The Young's modulus and Poisson ratio of the silicon chip are 169.5GPa and 0.278 respectively. The coefficient of thermal expansion of the silicon chip is 2.8ppm/°C. The FR-4 substrate is assumed to have an orthotropic property. The Poisson ratios ν_{xz}, ν_{xy} and ν_{yz} are 0.02, 0.143 and 0.143 respectively. The Young's moduli E_x, E_z and E_y are 22.4GPa, 22.4GPa and 1.6GPa respectively. The *CTEs* of FR-4, α_x, α_y and α_z are 16ppm/°C, 65ppm/°C and 16ppm/°C respectively (Auersperg, 1997). The x and y directions are defined in Figure 1. The z direction follows the right-hand rule.

In order to investigate the creep behaviors of solder joints and underfill for the flip chip specimen by different constitutive laws, six FEA models are considered as listed in Table 1. These include (1) both solder and underfill are considered as strain rate dependent plasticity (viscoplasticity); (2) the creep behaviors of both solder joint and underfill are described by hyperbolic power law; (3) the creep behavior of solder joint is still described by hyperbolic power law, but the underfill's by viscoelasticity; (4) the solder join is assumed to follow the strain rate-dependent visco behavior, but the underfill is described by elastic behavior, (5) both solder and underfill are considered as elastic and plastic materials; (6) both solder and underfill are considered as elastic materials.

Table 1 FEA model description

FEA model	Description
Case *I*	Strain rate dependent (solder and underfill)
Case *II*	Hyperbolic power law (solder and underfill)
Case *III*	Viscoelastic (underfill) Hyperbolic power law (solder)
Case *IV*	Elastic (underfill) Strain rate dependent (solder)
Case *V*	Elastic-plastic (solder and underfill)
Case *VI*	Elastic (solder and underfill)

The strain rate dependent properties of the underfill and the solder joints are described by:

$$\dot{\varepsilon}^{pl} = D\left(\frac{\bar{\sigma}}{\sigma^o} - 1\right)^p \quad for \quad \bar{\sigma} \geq \sigma^o, \qquad (1)$$

where $\dot{\varepsilon}^{pl}$ is the uniaxial equivalent plastic strain; $\bar{\sigma}$ is the yield stress at nonzero plastic strain rate; σ^o is the static yield stress; and D and p are material parameters.

Hyperbolic power law, which is commonly used to describe the viscoplastic behavior of material, is described as follows:

$$\dot{\varepsilon}^{cr} = A(\sinh B\sigma)^n \exp(-\Delta H / RT) \qquad (2)$$

where $\dot{\varepsilon}^{cr}$ is the uniaxial equivalent creep strain rate; σ the equivalent stress; ΔH the activation energy; R the universal gas constant; T the temperature; A, B and n some constants which are related to temperature and loading etc.

The viscoelastic model is based on the Maxwell model using a series combination of dashpot and spring element (Ferry 1980). The model was defined by the Prony series expansion:

$$G(t) = G_e + \sum_{i=1}^{N} G_i e^{-\frac{t}{\tau_i}} \qquad (3)$$

where G_e represents the equilibrium modulus, G_i and τ_i are the modulus and relaxation time for each element respectively. A total of 13 Maxwell elements are used in the study. For thermorheologically simple materials, the temperature effect was introduced through a reduced time concept. The reduced time, $\xi(t)$, was defined by

$$\xi(t) = \int_0^t \frac{d\tau}{a_T(T(\tau))} \qquad (4)$$

where a_T, the shift factor at time t, can be approximated by the Williams-Landel-Ferry (WLF) equation:

$$\log a_T = \frac{-C_1(T - T_r)}{C_2 + (T - T_r)} \qquad (5)$$

where T_r is the reference temperature. C_1 and C_2 are calibration constants obtained at this temperature.

The accuracy of finite element results strongly depends on the reliable input material database, in particular, consistent and precise experiment data. Therefore, a series of tests including tensile, creep and fatigue, are carried out on a computer controlled 6-axis mini fatigue tester for both eutectic solder alloy 63Sn37Pb and underfill FP4526 (Ren *et al.* 1997, Ren *et al.* 1998, Qian *et al.* 1998). The specimen used in the test is a specially designed thin strip specimen that has been verified to be suitable for the testing of solder alloys and underfills (Ren *et al.* 1997). The typical true stress-strain relationships and the creep test results of two materials are illustrated in Figure 4 ~ Figure 7. All the constant used in different FEA models can be determined from the test data.

EXPERIMENTS

Moiré interferometry is a whole-field in-plane displacement measurement technique with both high sensitivity and high spatial resolution. It is especially effective for the measurement of non-uniform in-plane deformation measurements (Post *et al*, 1993; Zou *et al.*, 1997). In this paper, real time moiré interferometry is applied to study the creep behavior of the flip-chip package. Figure 8 schematically shows the experiment setup.

The grating was replicated onto the surface of the same flip-chip package sample considered in FEM analysis at room temperature. Then the flip-chip specimen was subjected to thermal load from room temperature (23°C) to 115°C. Isothermal condition was maintained and was controlled at 115°C for about 10 hours and 40 minutes. The thermal deformations of the flip-chip package specimen in relation to temperature were measured. The fringe patterns were recorded by a CCD camera and stored into a PC computer in a digital format. In addition, the computer image processing technique was used to analyze the fringe patterns.

RESULTS AND DISCUSSIONS

Comparison of Results between FEA and Test

To compare the results between the finite element analysis and the test conducted by the real-time moiré interferometry, the steady state deformed configuration of the flip-chip package is selected, that is, the deformation state after 10 hours and 40 minutes creep at 115°C. The displacements at the prescribed location *A* on the specimen, as shown in Figure 9, obtained from the test and the finite element analysis are given in Table 2. It is found that the differences are less than 22%. It is shown that the displacements obtained from the finite element analysis for all FEA models are in agreement with those obtained from the test.

Table 2 Comparison of steady state displacements at *A* between FEA and moiré test (location *O* selected as reference point)

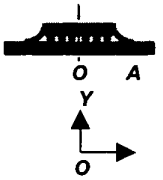

FEA model	Direction	Displacement (μm)	Difference (%)
Case *I* --Strain rate-dependent (solder and underfill)	*X* *Y*	7.04 4.28	20.55 2.64
Case *II*--Hyperbolic power law (solder and underfill)	*X* *Y*	7.05 4.54	20.72 8.87
Case *III*--Hyperbolic power law (solder), Viscoelastic (underfill)	*X* *Y*	7.0 3.25	19.86 -22.00
Case *IV*—Elastic (underfill), Strain rate dependent (solder)	*X* *Y*	6.98 4.29	19.52 2.88
Case *V*--Elastic-plastic (solder and underfill)	*X* *Y*	7.05 4.6	20.72 10.31
Case *VI*--Elastic (solder and underfill)	*X* *Y*	7.06 4.98	20.89 19.42
Test Results (μm)	*X* *Y*	5.84 4.17	- -

The typical displacement contours simulated by the finite element method and the fringe patterns captured by the moiré interferometry technique both in the *X* and *Y* directions are shown in Figure 10 and Figure 11. It is found that the configurations of the flip-chip package specimen captured by the moiré interferometry technique show the similar patterns compared with those modeled by the finite element method. In particular, the variation of the deformation predicted by the finite element method has the same trend as that obtained by the moiré test. Therefore, the FEA results are comparable to the test results.

Comparison of the displacements obtained by different FEA models

Figure 12 and Figure 13 show the variations of *X* and *Y* direction displacements at the location *A* with respect to the location *O* versus time for six different FEA models. From the results, it can be found that there is no obvious difference of displacements for different FEA models in which the material behaviors for solder and underfill are described by different constitutive models due to the constrained small volumes of the solder balls and underfill comparing with the whole flip-chip package specimen.

Furthermore, the displacements both in the *X* and *Y* direction do not change significantly during the temperature holding time. For example, the variation range of the *X* direction displacements is within the range of several manometers. For Case *I* — strain rate-dependent model (solder & underfill), the *X* direction displacement decreases from 7.0486μm to 7.0404μm during the temperature holding time. This means that the creep behavior of the underfill and the solder balls does not have significant effect on the warpage of the flip-chip under the considered thermal load.

Comparison of Von Mises stress in solder balls

In order to demonstrate the effect of the creep behavior of the underfill and the solder balls on the stresses in the solder balls, the Von Mises stress in the solder balls is analyzed. The results show that the highest Von Mises stress occurs at the corner of the outmost solder ball. Figure 14 shows the variations of Von Mises stress at the corner *B* of the outmost solder ball versus time predicted by different FEA models. The following results can be obtained.

1. As expected the Von Mises stresses predicted by elastic-plastic model-Case *V* and elastic model-Case *VI* are much higher than those of predicted by the models in which the visco behavior of the material is considered. At steady state, as described in the previous text, the values of Von Mises Stress at the corner of the outmost solder ball are one order of magnitude higher.

2. The stresses predicted by all visco models (Case *I* to Case *IV* as described in Table 1) are sharply reduced due to the creep behavior of solder balls. The stress relaxation occurs even in the heating stage.

3. For the prescribed location the stress values predicted by all visco models have no big difference. Furthermore, for all visco models the variations of the stresses versus time have the same trend.

In order to see if the above results are still available for all the locations in the solder ball, the Von Mises stress at the center ***D*** of the outmost solder ball is also analyzed. Figure 15 shows the variations of Von Mises stress at the center ***D*** of the outmost solder ball versus time predicted by different FEA models. It is observed that the Von Mises stress has the same trend as those at the corner ***B*** of the outmost solder ball.

Therefore, although the creep behavior of the solder balls and the underfill does not have significant effect on the warpage of the flip-chip, it does have a strong effect on the stresses in the solder balls.

Comparison of Von Mises stress in underfill

From the finite element study, it can be found that the highest Von Mises stress in the underfill occurs at the corner ***C*** as shown in Figure 9. The variations of Von Mises stress at corner ***C*** versus time predicted by different FEA models are given in Figure 16.

Like the Von Mises Stress in the solder ball, the creep behavior of solder balls and underfill sharply reduces the Von Mises stress at the corner ***C*** of underfill predicted by the visco models (case ***I*** to case ***III*** as described in Table 1). But it is very interested to find that the Von Mises Stress at corner ***C*** predicted by hyperbolic power law does not change during the temperature holding time. This is because that the creep behavior of underfill is dominated by first stage creep as shown in Figure 7. However, the hyperbolic power law is mainly used to describe the secondary stage and tertiary stage creep, which are usually the dominated creep stages such as the creep in solder alloy. Therefore, although the hyperbolic power law can well describe the creep behavior of solder alloy, it is not the case for underfill. In order to be able to well simulate the creep behavior of underfill, it is suggested to use the strain rate-dependent visco model.

Comparison of inelastic equivalent strain in solder ball and underfill

The inelastic equivalent strain $\bar{\varepsilon}$ can be obtained by

$$\bar{\varepsilon} = \sqrt{\frac{2}{3} e^i_{ij} e^i_{ij}} \qquad (6)$$

where $e^i_{ij} = \varepsilon^i_{ij} - \varepsilon^i \delta_{ij}$ and $\varepsilon^i = \frac{1}{3}(\varepsilon^i_{11} + \varepsilon^i_{22} + \varepsilon^i_{33})$.

ε^i_{ij} are the total inelastic components which can be obtained from ABAQUS output files.

Figure 17 shows the variations of inelastic equivalent strains at the corner ***B*** of the outmost solder ball. It seems that there is no significantly difference among the inelastic equivalent strains predicted by first three models, in which the materials for both the solder balls and the underfill are assumed to follow the visco behaviors. While ignoring the visco behavior of the underfill, the inelastic equivalent strain at the corner ***B*** of the outmost solder ball at the steady state increases up to 34.6% compared with the result from Case ***I*** in which both solder and underfill are described by strain rate-dependent constitutive model. If both the underfill and the solder are assumed to follow the elastic-plastic behaviors, that is, both of them do not follow the visco behaviors, the inelastic equivalent strain decreases up to 87.6% compared with the result form Case ***I***. It has the same trend for the inelastic equivalent strain at the center ***D*** of the outmost solder ball as shown in Figure 18. Usually the inelastic equivalent strain is used as main parameter for the fatigue life prediction. Therefore, it should be very careful to choose the suitable model in order to obtain accurate fatigue life prediction.

Figure 19 presents the variations of inelastic equivalent strains at the corner ***C*** of underfill. As expected, the inelastic equivalent strain obtained by hyperbolic power law shows the same trend as the Von Mises Stress, that is, the inelastic equivalent strain keeps unchanged during the temperature holding time. On the other hand, for another two visco models, strain rate-dependent (solder & underfill) model and viscoelastic (underfill) + hyperbolic power law (solder) model, the inelastic equivalent strain shows the similar results.

CONCLUSIONS

Based on the current study and current package, the following conclusions can be made:

1. The FEA results show that the predictions of the displacements for all models are in agreement with those obtained from the test. The differences between the displacements at the prescribed locations obtained from the finite element analysis and the test are below 22%. Therefore, the FEA results are comparable to the test results.
2. Solder and underfill nonlinear material models do not have significant effect on the warpage of the flip-chip under the considered thermal load condition, but do have significant effect on the stresses. For Von Mises stress at the corner or center of outmost solder ball predicted by all visco models sharply decreases. Whereas the Von Mises stresses predicted by elastic-plastic model and elastic model remain unchanged during the temperature holding time and are much higher.
3. Although the stress values predicted by all visco models for the solder ball at the prescribed locations have no big difference, it is not the case for underfill. To well simulate the creep behavior of underfill, it is suggested to use the strain rate-dependent visco model.
4. It seems that there is no significantly difference among the inelastic equivalent strains predicted by the FEA models, in which the materials for both the solder balls and the underfill are assumed to follow the visco behaviors. However, if the visco behaviors of both the solder and the underfill or only the visco behavior of the underfill is neglected, the inelastic equivalent strains in the solder ball have much difference. Therefore, it is suggested that the suitable model be carefully chosen in order to be able to obtain accurate fatigue life prediction.

ACKNOWLEDGMENTS

The authors would like to acknowledge the support of NSF PFF (Presidential Faculty Fellow) Award to S. Liu and SRC (Semiconductor Research Corporation).

REFERENCES

J. Auersperg, "Fracture and Damage Evaluation in Chip Scale Packages and Flip-Chip Assemblies by FEA and Microdac," ASME, Symposium on Applications of Fracture Mechanics in Electronic Packaging, Dallas, November 16-21, pp.133-138, 1997.

K. Darbha, J.H. Okura and A.Dasgupta, "Impact of Underfill Filler Particles on Reliability Of Flip Chip Interconnects," 1st IEEE International Symposium on Polymeric Electronics Packaging, PEP'97 Norrkoping, Sweden, 1997.

J. D. Ferry, "Viscoelastic Properties of Polymers," 3rd Edition, John Wiley & Sons, 1980.

V. Gektin, A. Bar-Cohen, and J. Ames, "Coffin-Manson Fatigue Model of Underfilled Flip-Chips," IEEE Trans. CPMT Part A. Vol. 20, No. 3, Sept. pp.317-326, 1997.

Bor Zen Hong, Tsomg-Dih Yuan and Lloy G. Burrell, "Anisothermal Fatigue Analysis of Solder Joints in a Convective CBGA Package Under Power Cycling," in Sensing, Modeling and Simulation in Emerging Electronic Packaging, ASME, EEP-Vol.17, 1996, pp.39-46.

J. H. Lau, "Flip Chip Technologies," McGraw-Hill, New York, 1996.

J. H. Lau and Yi-Hsin Pao, "Solder Joint Reliability of BGA, CSP, Flip Chip, and Fine Pitch SMT Assemblies," McGraw-Hill, New York, 1997

John H.L. Pang, Tze-Ing Tan and Suresh K. Sitaraman, " Thermo-Mechanical Analysis of Solder Joint Fatigue and Creep in a Flip Chip on Board Package Subjected to Temperature Cycling Loading," 48th Electronic Components and Technology Conference, Seattle, Washington, pp.878-883, 1998.

D. Post, B. Han, and P. Ifju, "High Sensitivity Moiré: Experimental Analysis for Mechanics and Materials," Springer-Verlag, NY, 1993.

Z. Qian, J. Yang and S. Liu, "Visco-Elastic-Plastic Properties and Constitutive Modeling of Underfills," 48th ECTC, Seattle, May 25-28, 1998.

W. Ren, Z. Qian, M. Lu, S. Liu and D. Shangguan, "Thermal Mechanical Properties of Two Solder Alloys," in Applications of Experimental Mechanics to Electronic Packaging, ASME, EEP-Vol.22, AMD-Vol.226, pp.125~130, 1997.

Wei Ren, Zhengfang Qian and Sheng Liu, "Thermo-Mechanical Creep of Two Solder Alloys," 48th Electronic Components and Technology Conference, Seattle, Washington, 1998 pp.1431-1437.

J. Wang, Z. Qian, D. Zou and S. Liu, "Creep Behavior of a flip-chip package by both FEM

Modeling and Real Time Moiré Interferometry," Transactions of the ASME, Journal of Electronic Packaging, Vol.120, No.2, 1998, pp.179-185.

Jie-Hua Zhao, Xiang Dai and Paul S. Ho, "Analysis and Modeling Verification for Thermal-mechanical Deformation in Flip-chip Packages," 48th Electronic Components and Technology Conference, Seattle, Washington, pp.336-344, 1998.

D. Zou, J. Wang, J. Zhu, M. Lu and S. Liu, "Creep Behavior Study of Plastic Power Package By Real Time Moiré Interferometry and FEM Modeling," ASME, Symposium on Applications of Experimental Mechanics to Electronic Packaging Dallas, November 16-21, 1997, pp.51-57.

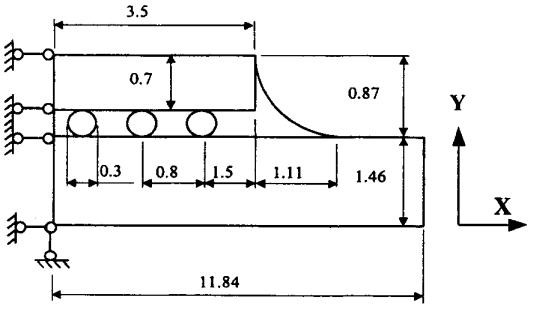

Figure 1 Dimensions and boundary conditions of flip-chip package

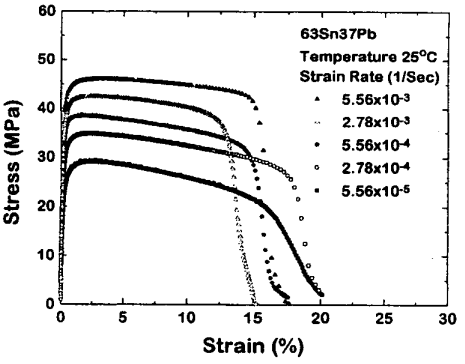

Figure 4 Typical stress-strain relationship of eutectic solder alloy 63Sn37Pb

Figure 2 Finite element mesh for flip-chip package

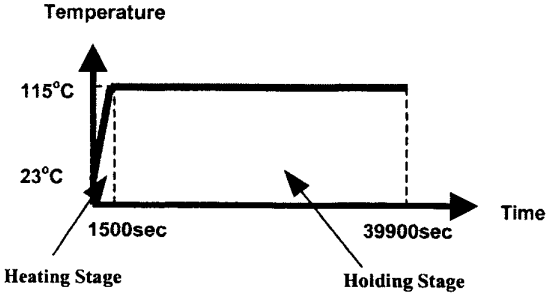

Figure 3 Temperature profile

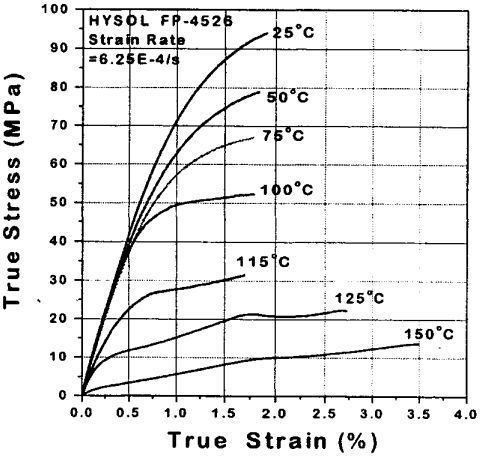

Figure 5 Typical stress-strain relationship of underfill FP-4526

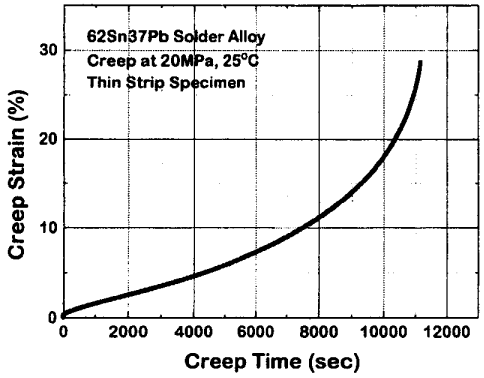

Figure 6 Typical creep test result of solder alloy

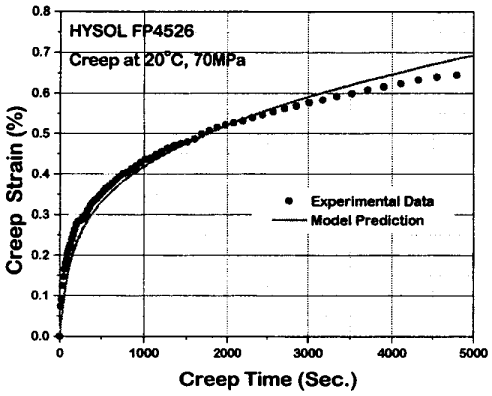

Figure 7 Typical creep test result of underfill

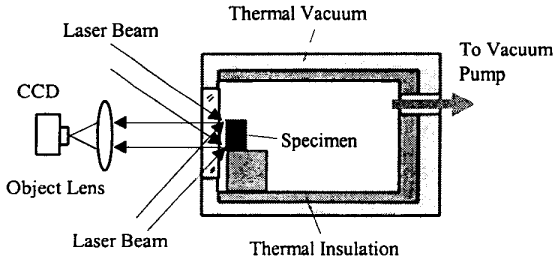

Figure 8 Schematic drawing of the test setup

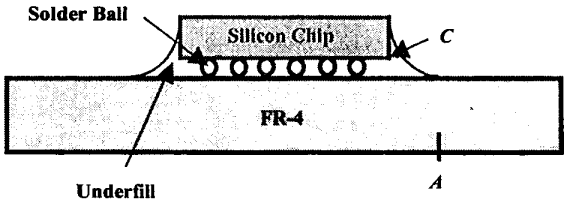

Figure 9 Flip-chip package specimen

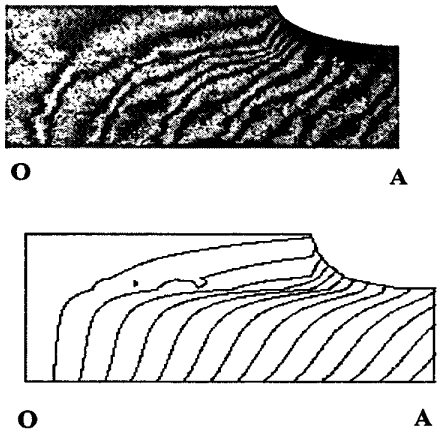

Figure 10 Steady state U-field (X direction) fringe patterns and FEM X direction displacement contours

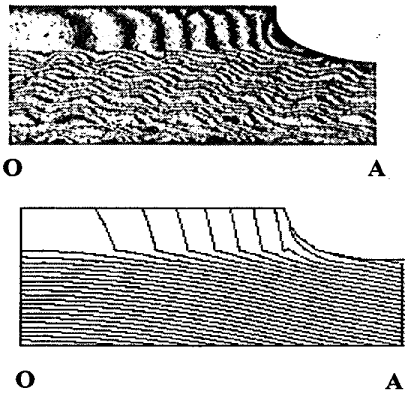

Figure 11 Steady state V-field (Y direction) fringe patterns and FEM Y direction displacement contours

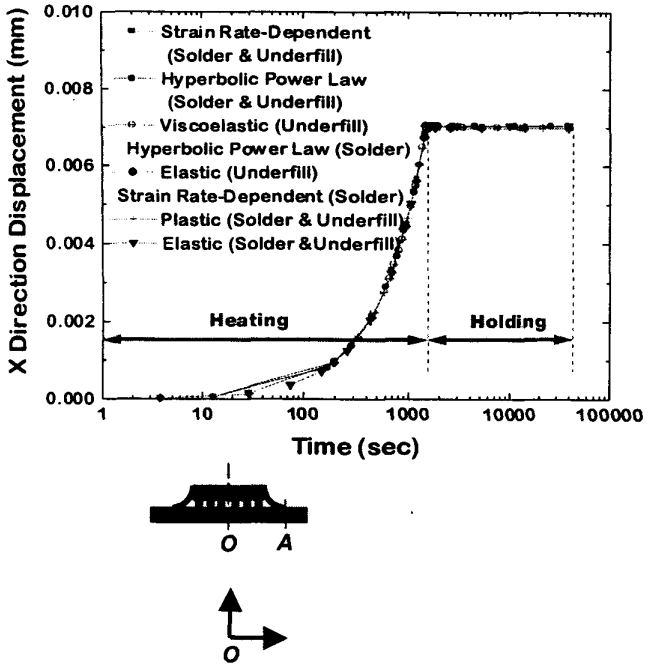

Figure 12 Variation of X-displacement at A with respect to O

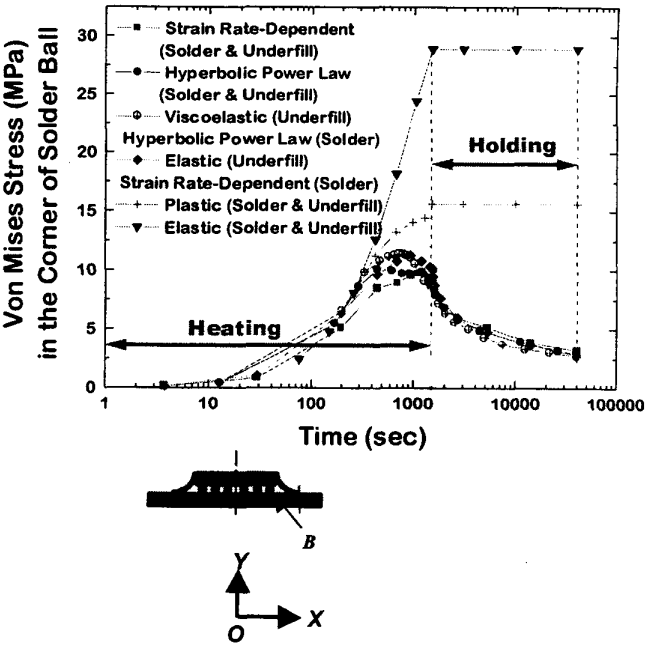

Figure 14 Variation of Von Mises Stress at the corner B of the outmost solder ball

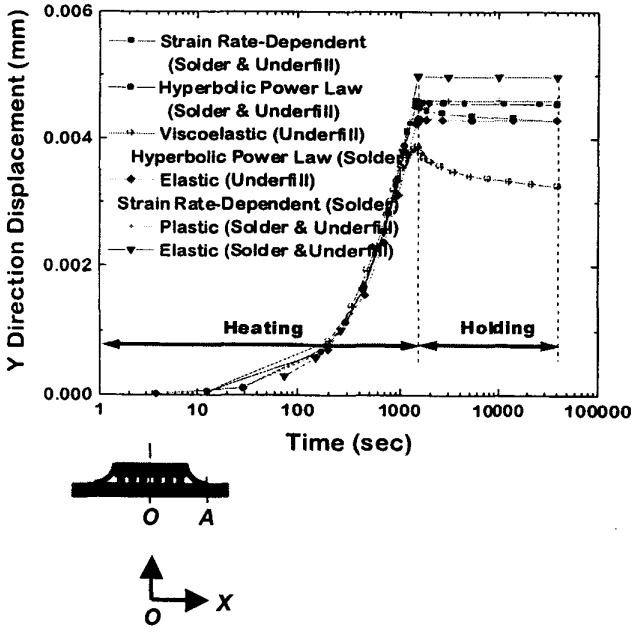

Figure 13 Variation of Y-displacement at A with respect to O

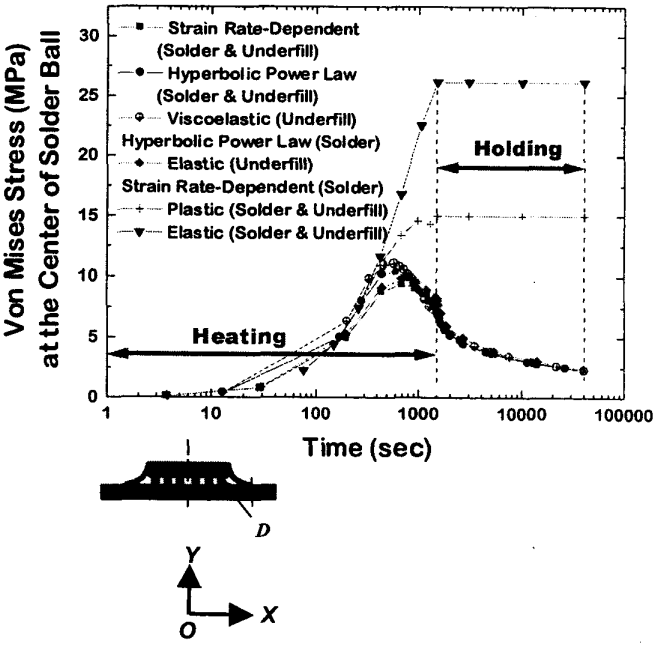

Figure 15 Variation of Von Mises Stress at the center D of the outmost solder ball

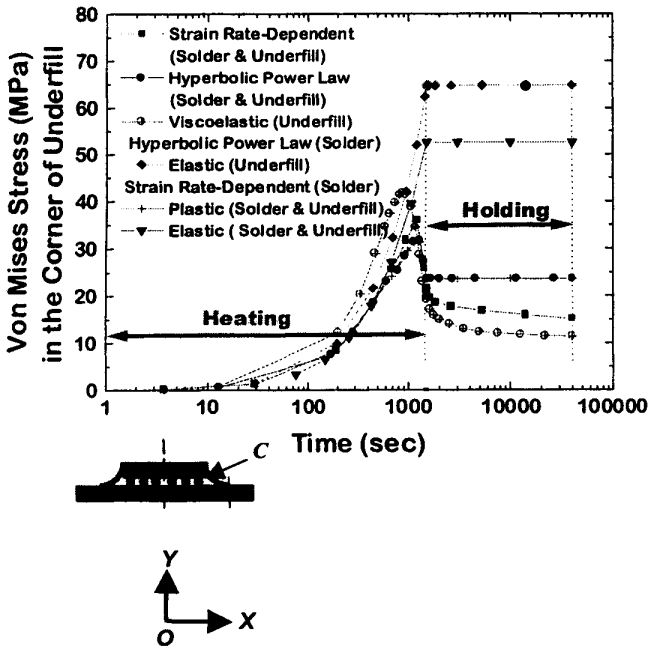

Figure 16 Variation of Von Mises Stress at the corner *C* of underfill

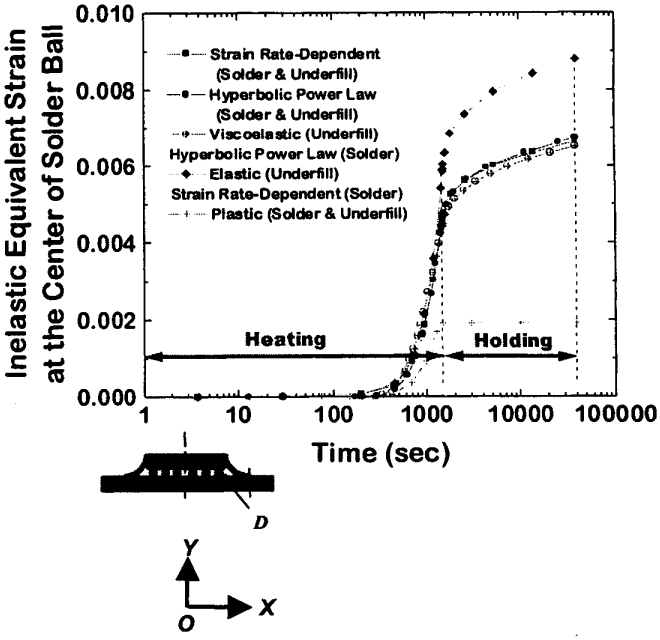

Figure 18 Variation of inelastic equivalent strain at the center *D* of the outmost solder ball

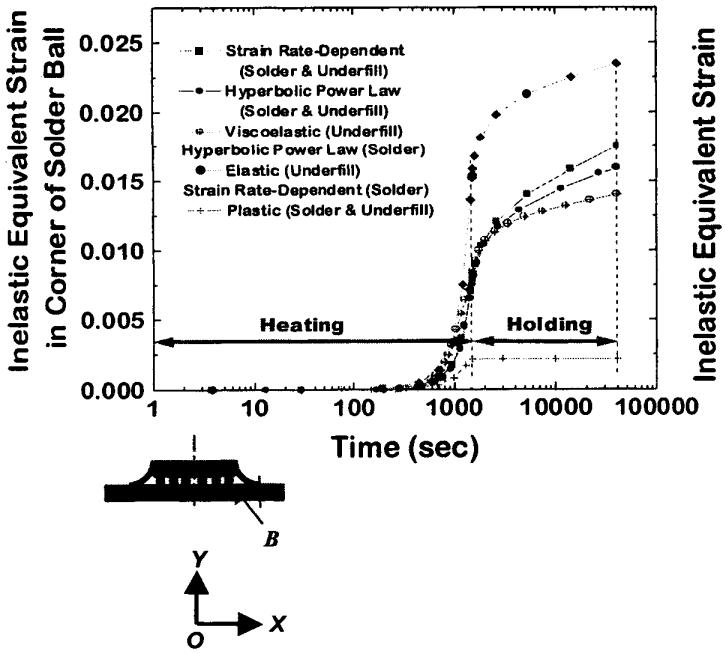

Figure 17 Variation of inelastic equivalent strain at the corner *B* of the outmost solder ball

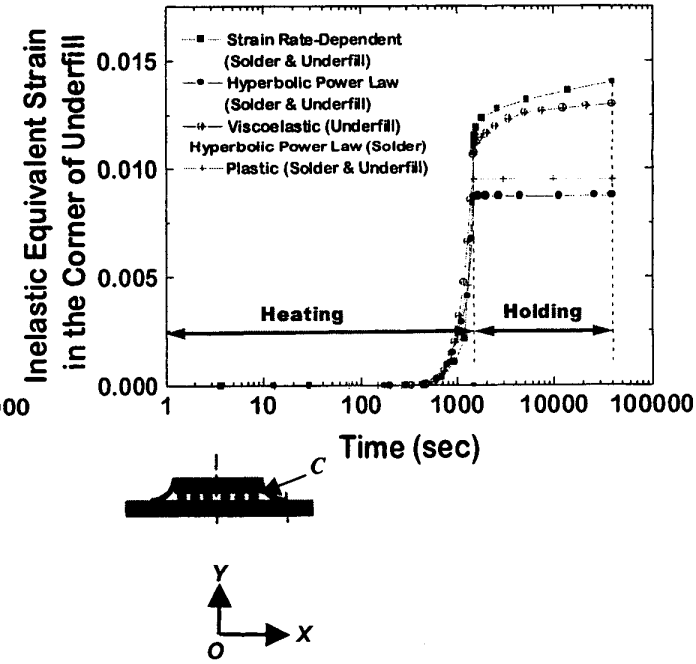

Figure19 Variation of inelastic equivalent strain at the corner *C* of underfill